JMEPEG (2023) 32:8593–8599
https://doi.org/10.1007/s11665-022-07745-w

1059-9495/$19.00

TECHNICAL ARTICLE

Cyclic Superelastic Behavior of Iron-Based Fe-Ni-Co-Al-Ti-Nb Shape Memory Alloy

C. Lauhoff, V. Remich, M.F. Giordana, C. Sobrero, T. Niendorf, and P. Krooß

Submitted: 29 July 2022 / Revised: 30 November 2022 / Accepted: 4 December 2022 / Published online: 3 January 2023

Iron-based shape memory alloys came into focus as promising candidate materials for large-scale structural applications owing to their cost-efficiency. In the present work, the superelastic properties of a recently introduced Fe-Ni-Co-Al-Ti-Nb shape memory alloy are investigated. For ⟨001⟩-oriented single-crystalline material in aged condition (650 °C/6 h), an incremental strain test reveals excellent superelasticity at −130 °C with fully reversible strains up to about 6%. Under cycling loading at different test temperatures, however, the alloy system investigated suffers limited functional stability.

Keywords heat treatment, nanoprecipitates, phase transformation, shape memory materials, superelasticity

1. Introduction

Since decades shape memory alloys (SMAs) are in focus of academia and industry owing to their unique functional properties. These are based on a thermoelastic, fully reversible phase transformation between a high-temperature austenitic parent phase and a low-temperature martensitic product phase. While the austenite features a high degree of crystallographic symmetry, the martensite is of lower symmetry. SMAs can provide for large reversible strains of up to about ∼ 10% and, thus, are promising materials for solid-state actuators and damping devices in various fields (Ref 1). Binary Ni-Ti is currently the most widely employed SMA system owing to its good functional properties, i.e., large transformation strains and superior structural as well as cyclic stability. Furthermore, Ni-Ti is highly biocompatible and can be processed into various semi-finished products (Ref 1, 2). Still, relatively high costs for alloying elements and complex processing limit its industrial usage to niche applications, in particular, in the biomedical sector (Ref 1).

In order to improve the cost efficiency, iron-based SMAs such as Fe-Ni-Co-based (Ref 3) and Fe-Mn-based systems (Ref 4) with low material costs and good cold workability are highly attractive and, thus, have received considerable attention in recent years. Following the development of Fe-Ni-Co-Ti SMAs, featuring only relatively low reversible transformation strains (2%) (Ref 5, 6), a Fe-Ni-Co-Al-Ta-B SMA was introduced in 2010 by Tanaka et al. (Ref 3), showing almost perfect superelasticity in polycrystalline state with high reversible strains of up to 13%. Fe-Ni-Co-Al-based alloys undergo a martensitic transformation (MT) from face-centered cubic (fcc) γ austenite to body-centered tetragonal (bct) α' martensite (Ref 3, 7). However, a prerequisite for the functional properties in newly developed Fe-Ni-Co-Al-based alloys is the presence of coherent nanoprecipitates, i.e., the $L1_2$-ordered γ'-phase with $(Ni,Fe,Co)_3(Al,X)$ composition (X = Ta, Nb or Ti), evoking a change from a non-thermoelastic to a thermoelastic character of the MT (Ref 3, 4, 7). By increasing the strength of the austenitic matrix via coherency stress fields, pronounced local plastic deformation via dislocation slip during MT is suppressed. Thereby, finely dispersed nanoprecipitates promote the reversibility of the MT and can reduce the temperature hysteresis by several hundred Kelvin (Ref 1, 5, 8). In addition, the nanoprecipitates increase the transformation temperatures by changing the matrix' chemical composition as an effect of Fe, Ni, and Co depletion (Ref 1, 7, 9).

Since nanoprecipitates are of utmost importance for the transformation characteristics, extensive work was conducted to study the influence of aging treatments on the functional properties in Fe-Ni-Co-Al-based SMAs. Ma et al. (Ref 7) found an aging treatment of 600 °C for 90 h to obtain 3.75% superelastic (SE) strain in single-crystalline Fe-Ni-Co-Al-Ta under tension. Spheroidal γ'-precipitates with diameters up to 5 nm were formed after this long aging time. In order to reduce the aging treatment time, replacing Ta by Ti is an effective approach. Fully reversible stress-strain responses with SE strains up to 6% were shown for Fe-Ni-Co-Al-Ti single crystals aged at 600 °C for only 4 h (Ref 10).

A Fe-Ni-Co-Al-Ti-Nb SMA and its SE properties are in focus of the present work. In Fe-Ni-Co-Al-based alloys, adding Nb has been reported to increase the strength of the austenitic matrix and, thus, improve the functional performance (Ref 11, 12). In recent years, first studies examined the fundamental microstructural and functional properties, i.e., the shape memory and SE behavior, of this novel iron-based SMA system (Ref 13-17). Maximum tensile SE strains were found to reach 6.7% in ⟨001⟩-oriented Fe-Ni-Co-Al-Ti-Nb single crystals (Ref 16).

Beside a thorough understanding of the phase transformation characteristics and the functional properties under mono-

C. Lauhoff, V. Remich, T. Niendorf, and **P. Krooß**, Institut für Werkstofftechnik, Universität Kassel, Mönchebergstr. 3, 34125 Kassel, Germany; **M.F. Giordana** and **C. Sobrero**, Institute of Physics Rosario-IFIR CONICET-UNR, Bv 27 de Febrero 210 Bis, 2000 Rosario, Argentina. Contact e-mail: lauhoff@uni-kassel.de.

tonic loading, it is mandatory to characterize the functional fatigue behavior under cyclic loading, since good cyclic stability is a key criterion for many envisaged applications of SMAs (Ref 1). In general, cyclic deformation can cause a significant change of the SE stress-strain hysteresis, which can result in a complete loss of the SE material response. This phenomenon is attributed to microstructural mechanisms rationalized by dislocation-slip, i.e., the introduction and accumulation of dislocations during the repeated phase transformation (Ref 1, 18-20). However, in Fe-Ni-Co-Al-Ti-Nb SMAs cyclic functional properties have not been addressed so far. To tackle this prevailing research gap, the current work primarily focused on the SE cyclic deformation behavior as a function of test temperature.

2. Experimental

Using billets melted from pure components large austenitic single crystals in the centimeter size range with a nominal chemical composition of Fe, 28% Ni, 17% Co, 11.5% Al, 1.25% Ti, and 1.25% Nb (at.%) were grown in helium atmosphere by Bridgeman method. Dog-bone-shaped tensile samples featuring a gauge dimension of $1.5 \times 1.6 \times 18$ mm^3 were electro-discharge machined (EDM) from the bulk single crystals with their load axes parallel to ⟨001⟩ of the austenitic phase. Single-crystalline tensile samples were prepared to reduce negative impact of grain boundaries on the functional properties. In order to remove any residue from machining, samples were mechanically ground down to 5 μm grit size. Homogenization and subsequent aging were conducted in sealed quartz glass tubes under argon atmosphere (to avoid oxidation) at 1300 °C for 24 h and 650 °C for 6 h, respectively, each followed by water quenching. To avoid issues related to deformation of the samples during the heat treatment procedures, samples were adequately supported within the quartz glass tubes. The homogenized samples were artificially aged to induce fine dispersed coherent γ'-nanoprecipitates, known to be crucially needed for a thermoelastic MT and functional properties. Aging parameters were chosen based on a series of preliminary tests. Among various aging treatments conducted in a wide range of aging temperatures and times, i.e., at 650-750 °C for 0.25-24 h, aging at 650 °C for 6 h leads to the best functional performance (cf. Fig. 1).

Mechanical testing was carried out on a servohydraulic test frame equipped with a 160 kN load cell, a temperature chamber and a liquid nitrogen heating/cooling system (KGW-Isotherm, Karlsruhe, Germany), enabling tests at temperatures from −150 to 100 °C. Quasi-static uniaxial incremental strain tests (ISTs) and cyclic experiments up to 100 SE cycles were performed in tension at various constant test temperatures. Temperatures were measured using a thermocouple directly attached to the sample. Tests were run in displacement control at a displacement rate of 0.015 mm s^{-1}. An extensometer with a gauge length of 12 mm (632.53F-14, MTS Systems Corporation, Eden Prairie, USA) was used for strain measurement. For preliminary mechanical characterization (cf. Fig. 1), in turn, displacement controlled uniaxial single cycle experiments were conducted at room temperature and at a displacement rate of 0.005 mm s^{-1} using a miniature load frame (Kammrath & Weiss, Germany) being capable of ± 10 kN. Strains were calculated from displacement data. In each cycle, a maximum nominal strain of 2% and a minimum load of 50 N were set for the loading and unloading path, respectively.

Microstructural analysis was conducted using a JEOL JEM-2100Plus transmission electron microscope (TEM). The TEM was operated at a nominal voltage of 200 kV. TEM samples were prepared by double-jet electro-polishing using a solution of 10% vol. perchloric acid in ethanol at −10 °C. In order to determine the characteristic transformation temperatures, electric resistance measurements were carried out using a liquid nitrogen heating/cooling system. Prismatic samples with dimensions of $1 \times 3 \times 20$ mm^3 were investigated at heating/cooling rates of 10 °C min^{-1}. Furthermore, hardness according to Vickers was determined with a hardness testing device using a load of 9.8 N.

3. Results and Discussion

Figure 2 shows the characteristic microstructure of Fe-Ni-Co-Al-Ti-Nb single-crystalline material following homogenization and subsequent aging treatment conducted at 650 °C for 6 h. In addition to the diffraction spots of the austenitic matrix (fcc), the selected area diffraction (SAED) pattern (Fig. 2b) obtained from the [011] zone axis reveals reflections (cf. white circle), which can be attributed to the γ'-phase (fcc unit cell with $L1_2$-ordering). As can be deduced from the dark field (DF)

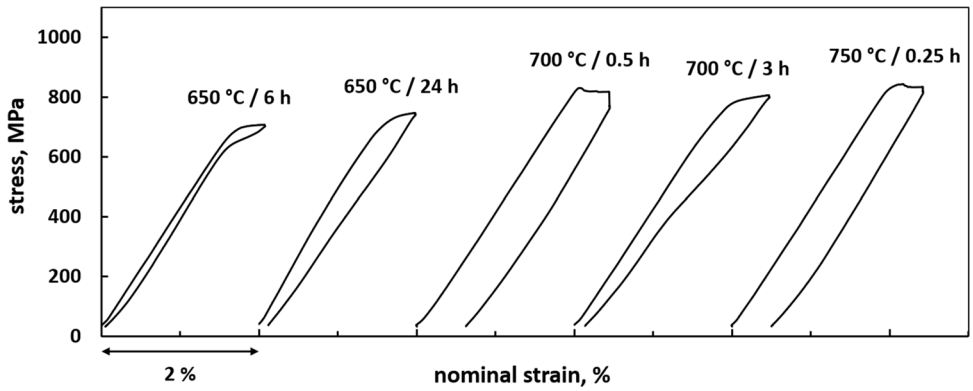

Fig. 1 SE stress-strain curves obtained under tensile load at room temperature for ⟨001⟩-oriented Fe-Ni-Co-Al-Ti-Nb single crystals following homogenization (1300 °C/24 h) and different aging treatments

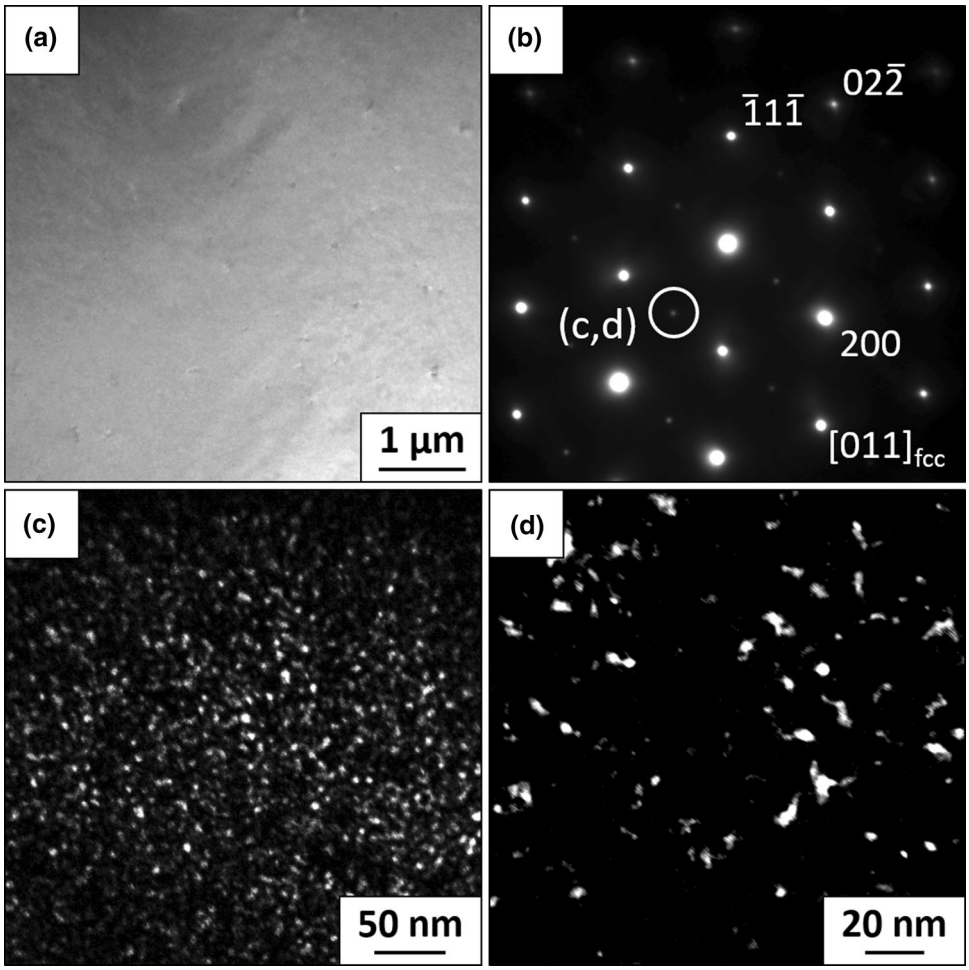

Fig. 2 TEM analysis of Fe-Ni-Co-Al-Ti-Nb revealing the microstructure following homogenization and aging at 650 °C for 6 h. TEM image (a) and corresponding SAED pattern (b) with reflection spots of the γ'-phase. DF images (c,d) obtained from the reflection spot encircled in (b) showing the morphology (size and shape) of γ'-precipitates (bright areas) formed after aging

images (Fig. 2c and d), the nanometric γ'-precipitates feature spheroidal shape with diameters up to 6 nm. The precipitate crystal structure and morphology (size and shape) reported in this study are fully consistent with data shown for long-time aging treatments (up to 72 h) at 600 °C in the Fe-Ni-Co-Al-Ti-Nb SMA system (Ref 13, 14).

In order to investigate the role of loading history on the reversibility of the stress-induced MT in ⟨001⟩-oriented Fe-Ni-Co-Al-Ti-Nb single crystals aged at 650 °C for 6 h, ISTs were conducted under tensile load at −130 °C. From the electrical resistance measurement in Fig. 3, it is obvious that the selected test temperature of −130 °C ensured a fully austenitic state prior to SE testing. No phase transformation upon cooling is visible in the resistivity curve, indicating a martensite start temperature (M_s) being below the temperature of liquid nitrogen. Fig. 4 shows a representative stress-strain curve. As can be deduced from the SE material response and the relation between reversible and applied strain (s. inset in Fig. 4), the sample exhibits a fully reversible stress-induced MT up to applied strain levels of 6% and a transformation strain (determined using the tangent method) of ∼ 4.0%. With further loading, however, the plastic yield stress of the stress-induced martensite is reached at around 950 MPa, as can seen from the

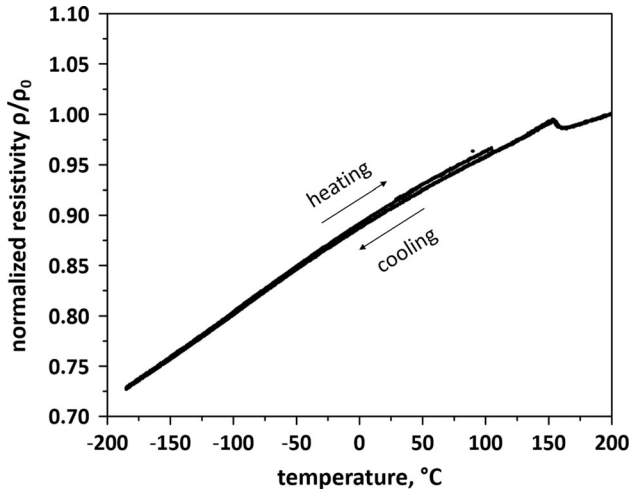

Fig. 3 Electrical resistance measurement of Fe-Ni-Co-Al-Ti-Nb following homogenization and aging at 650 °C for 6 h revealing no martensitic phase transformation upon cooling. The resistivity ρ is normalized to the resistivity measured at 150 °C (ρ_0)

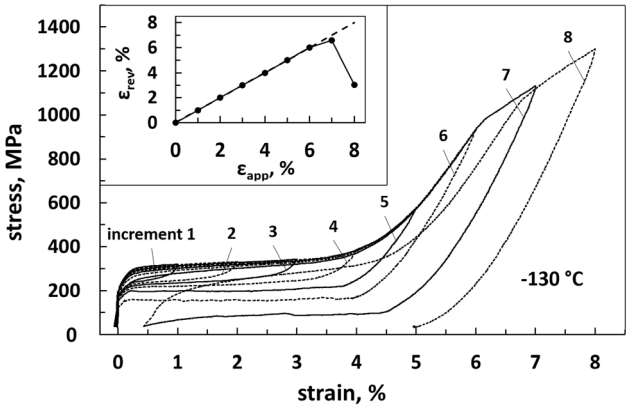

Fig. 4 SE stress-strain curve under tensile load at −130 °C for single-crystalline ⟨001⟩-oriented Fe-Ni-Co-Al-Ti-Nb aged for 6 h at 650 °C. The inset depicts the relation between reversible (ε_{rev}) and applied strain (ε_{app})

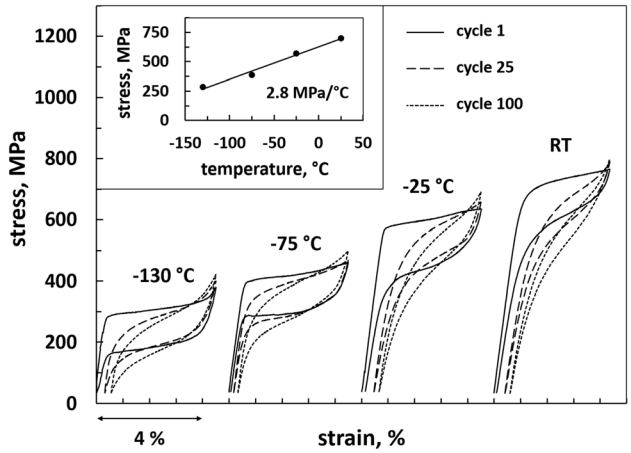

Fig. 5 SE cyclic stress-strain responses under tensile load at different test temperatures for single-crystalline ⟨001⟩-oriented Fe-Ni-Co-Al-Ti-Nb aged for 6 h at 650 °C. The inset reveals the Clausius-Clapeyron relationship

change of the stress-strain slope in the loading path. As a result of the onset of plastic deformation pronounced residual strains arise (s. Fig. 4) (Ref 1).

For the stress hysteresis ($\Delta\sigma$), defined as the difference between the stress of the loading and unloading plateaus, a slight increase is already visible within the first increments. A quite large value of about 160 MPa is reached after the 6th increment (s. Fig. 4). In general, non-chemical effects related to the accommodation of austenite and martensite structures are decisive for the hysteretic character of the MT (Ref 1). Employing in situ techniques, significant differences in the stress-induced transformation behavior between the loading and unloading path have been reported in various SMA systems (Ref 20-22). As well-known from literature, $\Delta\sigma$ is directly related to energy dissipating processes taking place during stress-induced MT. High values of $\Delta\sigma$ can be ascribed to: (1) high frictional work spent to overcome the resistance for phase boundary motion, (2) dissipation of stored elastic strain energy accumulated during the martensitic forward transformation, and/or (3) dissipation of interfacial energy (Ref 1, 23). Moreover, high values of $\Delta\sigma$ indicate ease of defect formation, e.g., dislocation formation during stress-induced MT (Ref 23). However, it should be emphasized that these defects do not affect the reversibility of the stress-induced MT within the first increments (cf. inset in Fig. 4). As already stated above, only when reaching the yield stress of martensite, residual strains can be seen. This is also consistent with the trend in the evolution of critical stress level (σ_{cr}), describing the nucleation stress, i.e., the onset, of the stress-induced MT upon loading: σ_{cr} remains nearly constant (around 300 MPa) irrespective of the applied strain until stress-induced martensite reaches the yield stress. In the subsequent cycles the accumulation of irreversibly deformed martensite may eventually lead to a decrease in σ_{cr}.

Figure 5 shows tensile cyclic SE stress-strain curves obtained at different test temperatures for ⟨001⟩-oriented single crystals in aged (650 °C / 6 h) condition. In each SE cycle, a fixed maximum tensile strain of 4.5% upon loading was set with respect to the transformation strain determined in the IST (Fig. 4). Results are shown for −130 °C,−75, −25 °C and room temperature (RT). At all test temperatures, an almost perfect SE material response is observed in each initial cycle. In turn, upon cyclic loading-unloading all Fe-Ni-Co-Al-Ti-Nb single crystals are characterized by an obvious change of the stress-strain behavior. A decrease in the critical stress level (σ_{cr}), a decrease in the stress hysteresis ($\Delta\sigma$), as well as an accumulation of residual strains are visible (Fig. 5). The degree in the cyclic functional degradation behavior, however, differs from temperature to temperature, i.e., increases with increasing test temperature (s. details below). Numerous studies over the last decades have proven that this cyclic evolution of the SE transformation characteristics is attributed to dislocation activities in the austenitic matrix (Ref 18-20, 24). In order to accommodate the mismatch between the austenitic and martensitic crystal structure, dislocation arrangements are known to be formed at the interphase boundaries during stress-induced MT (Ref 25). On the one hand, localized internal stress fields around these dislocations can stabilize the stress-induced martensite by providing mechanical energy, leading to an accumulation of residual strain. On the other hand, the internal stress fields promote the nucleation of martensite in subsequent cycles, causing the decrease of σ_{cr}. As the critical stress level for the reverse transformation remains almost unchanged upon cycling (s. Fig. 5), the decrease of $\Delta\sigma$ results from the decreasing values of σ_{cr} (Ref 20).

In order to quantitatively assess the cyclic stability of the stress-strain behavior for Fe-Ni-Co-Al-Ti-Nb SMA at a given test temperature, the evolution of σ_{cr} in relation to the 1st cycle of each fatigue experiment is plotted as a function of cycle number in Fig. 6(a). While in the early stages of cycling (up to 10 cycles) a quite rapid reduction of σ_{cr} is visible, the decrease of σ_{cr} slows down (at RT) or even nearly saturates (at −130 °C, −75, and −25 °C) with further cycling. Such cyclic saturation of the SE transformation characteristics, attributed to a steady-state dislocation structure (Ref 24), was numerously observed in various SMAs (Ref 18-20, 24). In total, the decrease of σ_{cr} steadily increases with test temperature. According to the steep Clausius-Clapeyron (CC) relationship of 2.8 MPa $°C^{-1}$ (s. inset in Fig. 5), the value of σ_{cr} increases from 285 MPa at −130 °C to 700 MPa at RT. Sobrero et al. (Ref 26) reported for the iron-based Fe-Ni-Co-Al-Ta SMA system that the degree of functional degradation increases with test temperature and correlates to how far the yield strength of

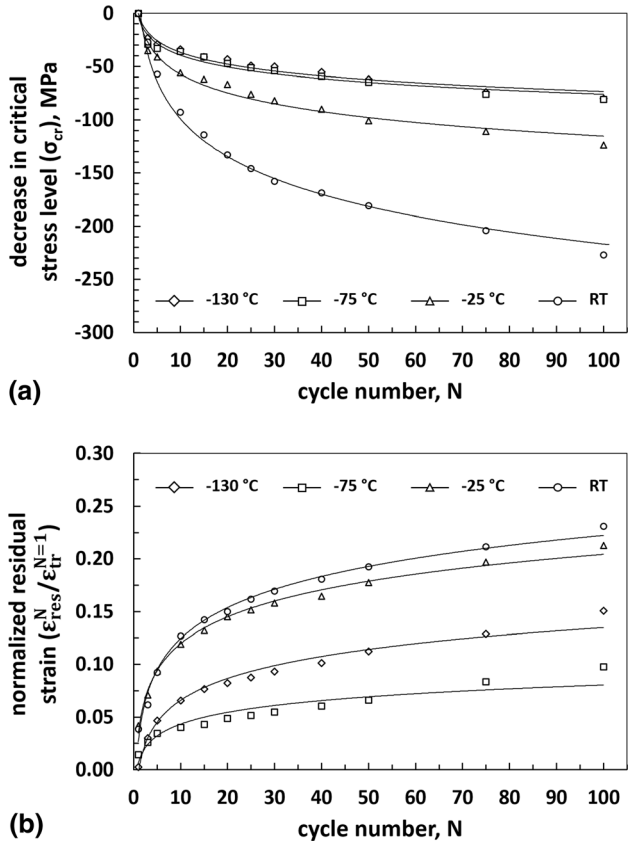

Fig. 6 Evolution of SE parameters versus cycle number for single-crystalline ⟨001⟩-oriented Fe-Ni-Co-Al-Ti-Nb aged for 6 h at 650 °C under SE cyclic tensile load at different test temperatures: (a) the decrease in critical stress (σ_{cr}), and (b) the residual strain after cycle number N (ε_{res}^{N}) normalized to the initial transformation strain of the 1st cycle ($\varepsilon_{tr}^{N=1}$). Data points were extracted from the results shown in Fig. 5

the material is exceeded at a given temperature. Thus, the temperature-dependent evolution of σ_{cr}, i.e., more pronounced changes of σ_{cr} during cyclic loading-unloading with increasing test temperature, is in perfect agreement with data shown in previous work (Ref 26). However, a direct correlation between the inherent width of the stress hysteresis ($\Delta\sigma$) and the fatigue performance, which was reported for Ni-Ti (Ref 27), Co-Ni-Ga (Ref 20) and Fe-Ni-Co-Al-Ta (Ref 28) SMAs, is not found in present work. The initial hysteresis in the 1st cycle (determined at half of the applied strain) is found to be 119, 125, 160, and 131 MPa at −130, −75, −25 °C, and RT, respectively (Fig. 5). While the sample tested at −25 °C features the largest stress hysteresis, it is obvious from Fig. 5 and 6 that testing at RT leads to the most pronounced changes in the cyclic stress-strain behavior. Thus, it seems to be that the critical stress level and its increase according to the CC relationship dominates the functional degradation of the Fe-Ni-Co-Al-Ti-Nb single crystals.

Another quantitative measure for cyclic degradation is illustrated in Fig. 6b. The accumulated residual strain is plotted for a given cycle number. For better comparability values are normalized to the initial transformation strain within the 1st fatigue cycle at each temperature. Since a constant absolute strain limit of 4.5% was considered in the cyclic experiments, contributions of strain being associated with the stress-induced MT and the elastic deformation of austenite changed from test temperature to test temperature. This is due to variations in σ_{cr} according to the CC relationship (cf. Fig. 5). As can be seen from the results presented in Fig. 6b, all single-crystalline samples suffer pronounced accumulation of residual strains upon cycling. In line with the evolution of σ_{cr} (Fig. 6a), the degree in residual strain accumulation increases with test temperature. Only the obviously and slightly improved recoverability of the sample tested at −75 °C compared to −130 °C deviates from this trend and cannot be explained so far. It has to be emphasized that this behavior, i.e., functional degradation occurring at all test temperatures, is in clear contrast to the Fe-Ni-Co-Al-Ta SMA, where excellent functional stability with perfect recoverability of the stress-induced MT upon cycling, i.e., no residual strain accumulation, was observed at −130 °C (Ref 26). Obviously, the Fe-Ni-Co-Al-Ti-Nb SMA in current state (aged at 650 °C for 6 h) features lower resistance against functional degradation, i.e., higher susceptibility for dislocation formation. With 390 HV_1 the hardness value is lower compared to 440 HV_1 obtained in ⟨001⟩-oriented Fe-Ni-Co-Al-Ta single crystalline material after aging at 700 °C for 1 h (Ref 29). Furthermore, it has to be noted that the precipitate morphology (size, shape and coherency) has a significant impact on the hardness of the microstructure and, thus, on irreversible processes (Ref 20, 27, 28, 30). For the Fe-Ni-Co-Al-Ta system, Ma et al. (Ref 7) and Krooß et al. (Ref 28, 29) reported the influence of different aging treatments on the precipitate structure, hardness and functional properties. With increasing aging time and precipitate size, for example, the width of the stress hysteresis ($\Delta\sigma$) increases, promoting pronounced cyclic instability (Ref 28). However, the complex interactions between the chemical composition and the precipitate morphology, explaining the lower hardness value of the aged (650 °C / 6 h) Fe-Ni-Co-Al-Ti-Nb condition than that in Ref. (Ref 29), cannot be clarified at this point. Such investigations require advanced techniques such as atom probe tomography and, thus, are beyond of the scope of present work.

4. Conclusions

In the present work, microstructure and superelastic (SE) properties were investigated for ⟨001⟩-oriented Fe-Ni-Co-Al-Ti-Nb shape memory alloy (SMA) single crystals in aged condition. The results obtained can be summarized as follows:

(1) TEM analysis reveals the formation of nanometric γ'-precipitates ($L1_2$-ordering) with spheroidal shape following homogenization and subsequent aging at 650 °C for 6 h.
(2) For this aging condition, incremental strain tests at −130 °C revealed excellent recoverability of the stress-induced martensitic transformation (MT) with transformation strains up to ∼ 4%.
(3) Irrespective of the applied test temperature, however, the Fe-Ni-Co-Al-Ti-Nb SMA suffers poor functional stability under SE cycling.

All in all, the present work reveals that the existing scientific knowledge about the microstructural and functional properties in the Fe-Ni-Co-Al-Ta SMA system seems not to be completely transferable to other alloy systems, that are characterized by slight compositional changes, i.e., substitution of 2.5% Ta by

1.25% Ti and 1.25% Nb (at.%). Whereas the Ta-alloyed SMA system shows perfect cyclic stability at lower temperatures, the Ti-Nb-alloyed material is characterized by functional degradation between room temperature and −130 °C. In particular, the impact of variations in local chemistry as well as changes in the local stress fields (coherency) in the vicinity of nanometric γ′-precipitates on the martensitic transformation and its stability upon cyclic loading is not fully understood so far and, thus, needs to be addressed in future studies.

Acknowledgments

This work was supported by Deutsche Forschungsgemeinschaft (DFG) [project No. 405372848 (KR 5134/1-1)]. Our partners are gratefully acknowledged for providing the single-crystalline material.

Funding

Open Access funding enabled and organized by Projekt DEAL.

Open Access

References

1. K. Otsuka Ed., *Shape Memory Materials*, 1st ed. Cambridge University Press, Cambridge, 1999
2. K. Otsuka and X. Ren, Physical Metallurgy of Ti-Ni-based Shape Memory Alloys, *Prog. Mater. Sci.*, 2005, **50**(5), p 511-678.
3. Y. Tanaka, Y. Himuro, R. Kainuma, Y. Sutou, T. Omori, and K. Ishida, Ferrous Polycrystalline Shape-Memory Alloy Showing Huge Superelasticity, *Science*, 2010, **327**(5972), p 1488-1490.
4. T. Omori, K. Ando, M. Okano, X. Xu, Y. Tanaka, I. Ohnuma, R. Kainuma, and K. Ishida, Superelastic Effect in Polycrystalline Ferrous Alloys, *Science*, 2011, **333**(6038), p 68-71.
5. H. Sehitoglu, I. Karaman, X.Y. Zhang, Y. Chumlyakov, and H.J. Maier, Deformation of FeNiCoTi Shape Memory Single Crystals, *Scr. Mater.*, 2001, **44**(5), p 779-784.
6. T. Maki, K. Kobayashi, M. Minato, and I. Tamura, Thermoelastic Martensite in an ausaged Fe-Ni-Ti-Co alloy, *Scr. Metall.*, 1984, **18**(10), p 1105-1109.
7. J. Ma, B.C. Hornbuckle, I. Karaman, G.B. Thompson, Z.P. Luo, and Y.I. Chumlyakov, The Effect of Nanoprecipitates on the Superelastic Properties of FeNiCoAlTa shape memory alloy single Crystals, *Acta Mater.*, 2013, **61**(9), p 3445-3455.
8. H. Sehitoglu, X.Y. Zhang, T. Kotil, D. Canadinc, Y. Chumlyakov, and H.J. Maier, Shape Memory Behavior of FeNiCoTi Single and Polycrystals, *Metall. Mat. Trans. A*, 2002, **33**(12), p 3661-3672.
9. K. Gall, H. Sehitoglu, Y.I. Chumlyakov, I.V. Kireeva, and H.J. Maier, The Influence of Aging on Critical Transformation Stress Levels and Martensite Start Temperatures in NiTi: Part I - Aged Microstructure and Micro-Mechanical Modeling, *J. Eng. Mater. Technol.*, 1999, **121**(1), p 19-27.
10. L.W. Tseng, J. Ma, I. Karaman, S.J. Wang, and Y.I. Chumlyakov, Superelastic Response of the FeNiCoAlTi Single Crystals Under Tension and Compression, *Scr. Mater.*, 2015, **101**, p 1-4.
11. Y.I. Chumlyakov, I.V. Kireeva, Z.V. Pobedennaya, P. Krooß, and T. Niendorf, Rubber-Like Behaviour and Superelasticity of [001]-Oriented FeNiCoAlNb Single Crystals Containing γ′- and β-Phase Particles, *J. Alloys Compd.*, 2021, **856**, 158158
12. Y.I. Chumlyakov, I.V. Kireeva, I.V. Kuksgauzen, D.A. Kuksgauzen, T. Niendorf, and P. Krooß, Tension-Compression Asymmetry of the Superelastic Behavior of High-Strength [001]-Oriented FeNiCoAlNb Crystals, *Mater. Lett.*, 2021, **289**, 129395
13. C.Y. Tsai, L.W. Tseng, Y.C. Tzeng, and P.Y. Lee, Magnetic Properties of FeNiCoAlTiNb Shape Memory Alloys, *Crystals*, 2022, **12**(1), p 121. https://doi.org/10.3390/cryst12010121
14. L.W. Tseng, Y.C. Tzeng, Y.L. Tsai, and Y. Chumlyakov, Microstructure Investigation of New Iron-Based FeNiCoAlTiNb Shape Memory Alloys, *Res. Mater.*, 2021, **10**, 100188
15. L.-W. Tseng, C.-H. Chen, W.-C. Chen, Y. Cheng, and N.-H. Lu, Shape Memory Properties and Microstructure of New Iron-Based FeNiCoAlTiNb Shape Memory Alloys, *Crystals*, 2021, **11**(10), p 1253. https://doi.org/10.3390/cryst11101253
16. Y. Chumlyakov, I. Kireeva, Z. Pobedennaya, I. Kuksgauzen, V. Poklonov, P. Krooß, T. Niendorf, C. Lauhoff, and M. Vollmer, Shape Memory Effect and Superelasticity in High-Strength FeNiCoAlTiNb Single Crystals, *In: Proceeding. International Conference (2020)*, p 20065
17. V. Poklonov, Y. Chumlyakov, I. Kireeva, and S. Lyamkin, Thermoelastic Martensitic Transformation in Single Crystals of FeNiCoAlTiNb Alloy, *AIP Conf. Proc.*, 2017, **1909**, p 20174.
18. S. Miyazaki, T. Imai, Y. Igo, and K. Otsuka, Effect of Cyclic deformation on the Pseudoelasticity Characteristics of Ti-Ni Alloys, *Metall. Mater. Trans. A*, 1986, **17**(1), p 115-120.
19. P. Krooß, C. Somsen, T. Niendorf, M. Schaper, I. Karaman, Y. Chumlyakov, G. Eggeler, and H.J. Maier, Cyclic Degradation Mechanisms in Aged FeNiCoAlTa Shape Memory Single Crystals, *Acta Mater.*, 2014, **79**, p 126-137.
20. C. Lauhoff, A. Reul, D. Langenkämper, P. Krooß, C. Somsen, M.J. Gutmann, B. Pedersen, I.V. Kireeva, Y.I. Chumlyakov, G. Eggeler, W.W. Schmahl, and T. Niendorf, Effects of Aging on the Stress-Induced Martensitic Transformation and Cyclic Superelastic Properties in Co-Ni-Ga Shape Memory Alloy Single Crystals Under Compression, *Acta Mater.*, 2022, **226**, 117623
21. J. Dadda, H.J. Maier, I. Karaman, and Y. Chumlyakov, High-Temperature in-Situ Microscopy During Stress-Induced Phase Transformations in $Co_{49}Ni_{21}Ga_{30}$ Shape Memory Alloy Single Crystals, *IJMR*, 2010, **101**(12), p 1-11.
22. A. Weidner, A. Vinogradov, M. Vollmer, P. Krooß, M.J. Kriegel, V. Klemm, Y. Chumlyakov, T. Niendorf, and H. Biermann, In Situ Characterization of the Functional Degradation of a [001] Orientated Fe-Mn-Al-Ni Single Crystal Under Compression Using Acoustic Emission Measurements, *Acta Mater.*, 2021, **220**, 117333
23. R.F. Hamilton, H. Sehitoglu, Y. Chumlyakov, and H.J. Maier, Stress Dependence of the Hysteresis in Single Crystal NiTi Alloys, *Acta Mater.*, 2004, **52**(11), p 3383-3402.
24. A. Yawny, M. Sade, and G. Eggeler, Pseudoelastic Cycling of Ultra-Fine-Grained NiTi Shape-Memory Wires, *Int. J. Mat. Res.*, 2005, **96**(6), p 608-618.
25. T. Simon, A. Kröger, C. Somsen, A. Dlouhy, and G. Eggeler, On the Multiplication of Dislocations During Martensitic Transformations in NiTi Shape Memory Alloys, *Acta Mater.*, 2010, **58**(5), p 1850-1860.
26. C. Sobrero, C. Lauhoff, D. Langenkämper, C. Somsen, G. Eggeler, Y.I. Chumlyakov, T. Niendorf, and P. Krooß, Impact of Test Temperature on Functional Degradation in Fe-Ni-Co-Al-Ta Shape Memory Alloy Single Crystals, *Mater. Lett.*, 2021, **291**, 129430
27. K. Gall and H.J. Maier, Cyclic Deformation Mechanisms in Precipitated NiTi Shape Memory Alloys, *Acta Mater.*, 2002, **50**(18), p 4643-4657.

28. P. Krooß, T. Niendorf, I. Karaman, Y. Chumlyakov, and H.J. Maier, Cyclic Deformation Behavior of Aged FeNiCoAlTa Single Crystals, *Funct. Mater. Lett.*, 2012, **5**(4), p 1250045.
29. P. Krooß, M.J. Holzweissig, T. Niendorf, C. Somsen, M. Schaper, Y.I. Chumlyakov, and H.J. Maier, Thermal Cycling Behavior of an Aged FeNiCoAlTa Single-Crystal Shape Memory Alloy, *Scr. Mater.*, 2014, **81**, p 28-31.
30. H. Sehitoglu, R. Anderson, I. Karaman, K. Gall, and Y. Chumlyakov, Cyclic Deformation Behavior of Single Crystal NiTi, *Metall. Mat. Trans. A*, 2001, **314**(1-2), p 67-74.